

OKLAHOMA STATE UNIVERSITY

MEASUREMENT OF THE ELASTIC MODULUS IN
COLLOIDAL CRYSTALS USING A BRAGG
SCATTERING TECHNIQUE

By

GREGORY LEE TRELEVEN

Bachelor of Science

Oklahoma State University

Stillwater, Oklahoma

1992

Submitted to the Faculty of the
Graduate College of the
Oklahoma State University
in partial fulfillment of
the requirements for
the Degree of
MASTER OF SCIENCE
August, 1997

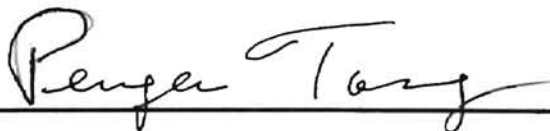
MEASUREMENT OF THE ELASTIC MODULUS IN
COLLOIDAL CRYSTALS USING A BRAGG
SCATTERING TECHNIQUE

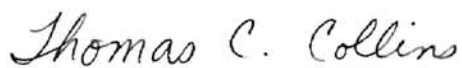
Thesis Approved:



Thesis Adviser







Dean of the Graduate College

ACKNOWLEDGEMENTS

At this time I would like to take a moment to thank all those who have made this thesis possible.

First of all, I want to thank my adviser, Prof. Bruce J. Ackerson, for allowing me the opportunity to work in his laboratory and for the help and advice he has given to me over the years. Working for him has been a great learning experience. Next, I want to thank my committee members Prof. Penger Tong and Prof. Larry Scott.

The guys in the laboratory have been a great help. Mr. Ulf Nobbmann has gone out of his way many times to help with all the the little problems that always seem to appear and Mr. Keith Davis has been very helpful with various data fitting programs. Thanks to all my friends and classmates for helping me pull through the hard times.

I would like to thank my parents for all of their love and encouragement.

And finally, I would like to thank my wife, Reagan, for encouraging me to continue with my work, and for putting up with me while I worked on this thesis.

TABLE OF CONTENTS

Chapter	Page
I. INTRODUCTION	1
II. THEORETICAL	4
Solving the elasticity equation	4
Derivation of an expression for resonance frequencies	5
III. EXPERIMENTAL PROCEDURES	8
Sample preparation	8
Experimental Setup	8
Position Sensitive Detector and amplification circuit	9
HP Analyzer and output data format	9
Testing the setup	10
IV. RESULTS	12
Discussion of accuracy and reliability of resonance detection methods	12
Discussion of data fitting and results	12
V. CONCLUSIONS	17
BIBLIOGRAPHY	18
APPENDICES	19
APPENDIX A - Amplification Circuitry	20
APPENDIX B - Theoretical Shear Modulus	21

LIST OF FIGURES

Figure		Page
1	Experimental Setup	9
2	Mechanical Resonance	11
3	Sensing Error	11
4	Typical Resonance Spectrum	13
5	Resonance Amplitude Data Fit	14
6	Elastic Modulus vs. Volume Fraction	15
7	Number of Screening Ions for FCC Polystyrene	15
8	Number of Screening Ions for BCC Polystyrene	16
9	Circuit Diagram	20

CHAPTER I

INTRODUCTION

Much interest has been shown in recent years in the study of colloidal systems. This is due in part to the fact that the lattice spacing of these spontaneously crystalized systems of charged macromolecules is comparable to the wavelength of visible light. As a result of this, laser light can be used to collect data from these crystalline arrays of suspended particles, as opposed to the x-ray illumination required in probing atomic crystals.

Several groups have devoted research to the measurement of the properties of colloidal dispersions, such as polystyrene, polymethyl methacrylate, and silica spheres, in a variety of solvents[1-7]. These properties include the shear modulus, as well as dynamic viscosity and sample structure and morphology. Methods of measurement have varied from rheologic measurements for highly concentrated samples, to light scattering rheological techniques for dilute samples. While it is impossible to detail within this paper all of the work done on this subject, it would perhaps be appropriate at this time to mention a few of the developments in the measurement of the elastic moduli of colloidal crystals.

Theoretical and experimental studies have been done by R. Nossal and M. Jolly to determine the allowable frequencies of the mechanically excited shear waves of soft gels in cylindrical cuvettes[8]. By solving a set of modified elasticity equations, they were able to show how the measured frequencies depended both on the material properties of a sample and on the dimensions of the sample's container. Using the observed resonances during inelastic light scattering, they were able to calculate the transverse sound speed and from that, the shear modulus of a sample.

In another work, a simple model based on the pair potential for interacting particles in a dilute electrolyte solution is used by R. Buscall *et al.*, as the basis for a comparison with experimental shear modulus data[1]. Using a rheometric apparatus, measurements of shear modulus were taken for polystyrene samples ($a=34.3$ nm) over a volume fraction range of $0.146 < \phi < 0.303$. The shear modulus data was seen to have increased smoothly from 280 Nm^{-2} at $\phi = 0.146$ to 3450 Nm^{-2} at $\phi = 0.303$. This shear modulus data was then fitted to the pair potential model to obtain an experimental value for a diffuse layer potential.

W. B. Russel and D. W. Benzing have developed a self consistent field theory that can predict the equilibrium and transport properties of ordered monodisperse lattices[10,11]. The multiparticle electrostatic interactions are used to calculate the osmotic pressure and the shear modulus. These depend on the volume fraction, the surface charge density, and the electrolyte concentration. The theory points out the role of the counterions in shielding the surface charge.

Advanced preparation and deionization methods have been developed by T. Palberg *et al.* in order to increase the accuracy and precision of shear modulus measurements[3]. The authors prepared BCC crystalline samples using polystyrene spheres of radius $a = 51 \text{ nm}$ at low volume fractions ($\phi = 0.01$). Two different methods were used to deionize the sample. In the first method, known as standing preparation, a small amount of mixed bed ion exchange resin is introduced into the cell containing the crystalline sample. A fine mesh is used to cover the resin beads and insure the flat lower boundary needed for the experiment. When using this method of deionization, great care must be taken to prevent contamination of the sample by airborne CO_2 . In the second method, known as continuous deionization, the suspension flows through a teflon tube system connected to an ion exchanger cell. Using this method of preparation, uncertainties in volume fraction and salt concentration were reported to be below 1%.

A Bragg scattering experimental set-up was used by T. Palberg *et al.* that involves a cylindrical cell mounted on a driven system consisting of an excentrically coupled loud speaker driven by a frequency generator[3]. A laser beam scatters off

a small crystallite in the center of the cell and is incident upon a position sensitive photodiode under an angle that satisfies the Bragg condition. Additionally, some measurements were taken by the authors in which a mirror was centered on the suspension interface of a sample prepared with free upper inert gas boundary.

In the following thesis, we begin by looking at the solution to the elasticity equations for an isotropic elastic medium as outlined by R. Nossal and M. Jolly[8]. From these equations, we can find the relationship between the resonance frequencies $\omega_{l,n}$ observed in a sample and the allowable normal modes $k_{l,n}$ for a cylindrical cell. From this relationship, the elastic modulus G can be calculated for any observed resonances. Next, the preparation and deionization of several samples using 0.107 micron diameter polystyrene and mixed bed ion-exchange resin is discussed. Construction and testing of the Bragg scattering experimental setup is reviewed. Data is taken and the experimental values for elastic modulus are compared with a pair potential model to determine an experimental value for the number of screening ions per polystyrene sphere. Finally, the values of the data obtained in this experiment are compared with those of other works.

CHAPTER II

THEORETICAL

Solving the elasticity equation

Although a sample will contain many microcrystallites, macroscopically it behaves as an isotropic elastic medium[4]. The elasticity equations for a crystalline sample can therefore be written as[9]

$$\rho \frac{\partial^2 \mathbf{U}}{\partial t^2} = \text{Div} \sigma + \mathbf{F}, \quad (1)$$

where ρ is the mass density of the sample, \mathbf{U} is the displacement vector of the sample, σ is a generalized stress tensor, and \mathbf{F} is the vector of applied forces. For small torsional excitations of a sample in a cylindrical cell, the applied field will have no angular dependence. Thus Eq. (1) reduces to the following set of equations[8]

$$\begin{aligned} \rho \frac{\partial^2 U_r}{\partial t^2} = & \left[(O_\lambda + 2O_\mu) \left(\frac{\partial^2 U_r}{\partial r^2} + \frac{1}{r} \frac{\partial U_r}{\partial r} - \frac{U_r}{r^2} \right) \right. \\ & \left. + (O_\lambda + O_\mu) \frac{\partial^2 U_z}{\partial r \partial z} + O_\mu \frac{\partial^2 U_r}{\partial z^2} \right] + F_r(r, z; t), \end{aligned} \quad (2)$$

$$\rho \frac{\partial^2 U_\theta}{\partial t^2} = O_\mu \left(\frac{\partial^2 U_\theta}{\partial r^2} + \frac{1}{r} \frac{\partial U_\theta}{\partial r} - \frac{U_\theta}{r^2} + \frac{\partial^2 U_\theta}{\partial z^2} \right) + F_\theta(r, z; t), \quad (3)$$

$$\begin{aligned} \rho \frac{\partial^2 U_z}{\partial t^2} = & \left[(O_\lambda + O_\mu) \left(\frac{1}{r} \frac{\partial^2 (r U_r)}{\partial r \partial z} \right) + (O_\lambda + 2O_\mu) \frac{\partial^2 U_z}{\partial z^2} \right. \\ & \left. + O_\mu \left(\frac{\partial^2 U_z}{\partial r^2} + \frac{1}{r} \frac{\partial U_z}{\partial r} \right) \right] + F_z(r, z; t), \end{aligned} \quad (4)$$

where U_r , U_θ , and U_z are the gel or suspension displacements along the radius, angular direction, and axis respectively. O_λ and O_μ are linear operators defined as[12]

$$\begin{aligned} O_\lambda f(t) &= \lambda f(t) + \int_{-\infty}^t \mathcal{L}(t-t') \frac{\partial}{\partial t'} f(t') dt', \\ O_\mu f(t) &= \mu f(t) + \int_{-\infty}^t \mathcal{G}(t-t') \frac{\partial}{\partial t'} f(t') dt', \end{aligned} \quad (5)$$

where $f(t)$ is an arbitrary function of time, λ and μ are the usual static Lamé coefficients, and $\mathcal{L}(t)$ and $\mathcal{G}(t)$ are kernels which decay to zero at long times.

Equations (2) and (3) show coupling between U_r and U_z . The applied forces and the boundary conditions will determine whether the resulting waves will be shear or compressional. Eq. (3) shows that U_θ is decoupled from U_r and U_z and will be related only with shear waves. In order to solve Eq. (3), we must consider the appropriate boundary conditions. Since the cell is undergoing only small excitations, we can assume that the sample sticks to the cell walls. If this is the case, then the boundary conditions are[8]

$$\begin{aligned} U_\theta(R, z; t) &= 0, r = R, \\ U_\theta(r, 0; t) &= U_\theta(r, h; t) = 0, z = 0, h. \end{aligned} \quad (6)$$

While these boundary conditions indicate that the top as well as the bottom of the sample is immobilized by the surface of the cell, in fact, the top of the sample is free to move. This discrepancy will be dealt with later.

Derivation of an expression for resonance frequencies

Assuming a cell excitation $g_\theta(t)$ which is a periodic twist of small amplitude and is of low frequency, it is clear that the body force $F_\theta(r, z, t)$ depends only on the time derivatives of $g_\theta(t)$. This must be since if the cell was turned very slowly, the entire sample would follow as well. In other words, for slow excitations $U(r, t)$ approaches zero. Since rotations at a steady velocity would not result in sample displacement, the lowest time derivative must be of first order and since

the displacements are small and of low frequency the lowest order term is most likely the only one of importance. The internal force can then be taken to be [8]

$$F_\theta(r, z; t) = \bar{\zeta} \frac{\rho r}{R} \frac{dg_\theta(t)}{dt}, \quad (7)$$

where $\bar{\zeta}$ is an unknown coefficient which likely varies with sample viscosity. If applied forces and internal dissipation are ignored ($g_\theta \equiv 0, O_\mu \rightarrow \mu$), the solution to Eq. (3) is

$$U_{l,n}(r, z; t) = J_1\left(\frac{\nu_l r}{R}\right) \sin \frac{n\pi z}{h} \exp^{i\omega_{l,n}t}, \quad (8)$$

where $J_1(\bullet)$ is a first order Bessel function of the first kind. ν_l are the zeros of $J_1(\bullet)$ and n is an interger. $\omega_{l,n}$ are frequencies given as $\omega_{l,n} = k_{l,n}C_{tr}$ where C_{tr} is the transverse sound velocity $C_{tr} = (G/\rho)^{1/2}$. The wavenumbers $k_{l,n}$ for cylindrical cuvettes are

$$k_{l,n} = \left(\left[\frac{\nu_l}{R} \right]^2 + \frac{n^2\pi^2}{h^2} \right)^{1/2}. \quad (9)$$

To solve Eq. (3) with the applied forces and internal dissipation, we anticipate a solution of the form

$$U_\theta(r, z; t) = \sum_{l=1}^{\infty} \sum_{n=1}^{\infty} a_{l,n}(t) J_1\left(\frac{\nu_l r}{R}\right) \sin \frac{n\pi z}{h}. \quad (10)$$

Where $a_{l,n}$ is given by

$$\frac{d^2 a_{l,n}}{dt^2} = -\frac{1}{\rho} k_{l,n}^2 O_\mu(a_{l,n}) + f_{l,n}(t), \quad (11)$$

where $f_{l,n}(t)$ is defined as

$$f_{l,n}(t) = \frac{4\bar{\zeta}}{\pi} n \nu_l J_2(\nu_l)^{-1} [1 - (-1)^n] \frac{dg_\theta}{dt}. \quad (12)$$

Eq. (11) can be solved formally for any arbitrary kernel $\mathcal{G}(t)$ appearing in Eq. (5). However, for this experiment we can assume that the relaxation of the sample occurs much faster than the frequency of oscillation of U_θ . We can thus approximate $\mathcal{G}(t)$ as

$$\mathcal{G}(t) \approx \eta \delta(t), \quad (13)$$

where η is a viscosity coefficient, $\delta(t)$ is a Dirac delta function, and the operator O_μ becomes

$$O_\mu \approx \mu + \eta \frac{\partial}{\partial t}. \quad (14)$$

If $g_\theta(t)$ is a periodic function given by $g_\theta(t) = g_0 \sin \omega t$, then ignoring initial value terms which decay to zero, the solution of Eq. (11) is [8]

$$a_{l,n}(t) = \frac{4\omega g_0 [1 - (-1)^n] \bar{\zeta}}{n\pi \nu_l J_2(\nu_l)} \times [(\omega^2 - k_{l,n}^2 C_{tr}^2)^2 + k_{l,n}^4 \eta^2 \omega^2 / \rho^2]^{-1/2} \times \sin(\omega t + \phi - \pi), \quad (15)$$

where η is a viscosity parameter and ϕ is the phase shift as given by

$$\tan \phi = \frac{\rho(k_{l,n}^2 C_{tr}^2 - \omega^2)}{\omega k_{l,n}^2 \eta}. \quad (16)$$

The maxima of the amplitudes in Eq. (15) occur at values of ω given by

$$\omega_m = k_{l,n} \sqrt{C_{tr}^2 - \frac{k_{l,n}^2 \eta^2}{\rho^2}}. \quad (17)$$

Since $k_{l,n}^2 \eta^2 / \rho^2$ is expected to be (and will later be shown to be) much smaller than C_{tr}^2 , ω_m can be approximated as

$$\omega_m \approx k_{l,n} C_{tr}. \quad (18)$$

The result of the top of the sample not being restrained as suggested in the boundary conditions is that Eq. (9) must be modified so that the values of n are no longer integers but half integers. Eq. (9) then becomes

$$k_{l,n} = \left(\left[\frac{\nu_l}{R} \right]^2 + \frac{(2n+1)^2 \pi^2}{4h^2} \right)^{1/2}. \quad (19)$$

Since the wavelengths of the allowable normal modes are dependent on the size of the sample cell, any changes in the sample cell dimensions R and h will result in a change in the observed resonance frequencies.

CHAPTER III

EXPERIMENTAL PROCEDURES

Sample preparation

Several samples were prepared using commercially available (Lot #16203 Duke Scientific) 0.107 micron diameter polystyrene spheres. In order to prevent aggregation due to van der Waals attraction, the particles are synthesized with a net charge to provide a stabilizing coulomb repulsion [6]. The polystyrene was mixed with purified, deionized ($18M\Omega$) water in concentrations ranging from 1.45×10^{-3} to 4.44×10^{-3} volume fractions and placed in cylindrical cells. Since highly ionic solutions will disrupt the charge on the spheres, mixed bed ion-exchange resin (analytical grade 20-50 mesh fully regenerated #27180 from Bio-Rad) is placed in the cuvette. This is done to minimize the ionic strength of the sample and maximize the interparticle repulsion.

Experimental Setup

A polystyrene sample in a cylindrical cuvette is centered on a turntable driven by an excentrically coupled loudspeaker (Figure 1). A helium-neon laser illuminating the crystalline sample results in Bragg scattering. As the speaker is driven with a sinusoidal signal from a frequency generator, the turntable and hence the crystalline sample experience a periodic torsional displacement. Shear waves are induced in the sample, and within the limit of small oscillations, the resulting sinusoidal shearing of the crystal corresponds to an equally sinusoidal variation in the Bragg angle. A position sensitive photodiode then detects the motion of one of these Bragg spots.

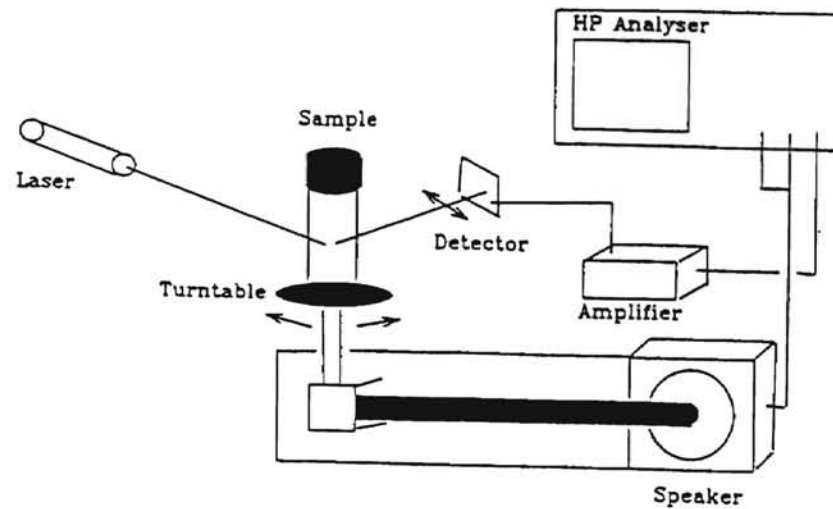


Figure 1. Experimental Setup: A speaker and turntable are used to excite torsional waves within a sample. A laser illuminates the sample and a detector measures the movement of a crystal which is oriented under Bragg conditions. The detectors signal is amplified and recorded on the analyser.

Position Sensitive Detector and amplification circuit

The movement of the Bragg spots was followed using an analog super linear position sensing detector (DL20 from UDT Sensors, Inc.). With a 4 square centimeter sensing area, the resolution of the detector is limited only by the signal amplification circuitry and the light source. According to the manufacturer, the position detection error over most of the sensing area is typically 20 microns with a maximum of 100 microns. The amplification circuitry (see Appendix A) translates and amplifies the raw signal from the sensor into an absolute position with respect to the center of the detecting surface.

HP Analyzer and output data format

The function generator on an HP Dynamic Signal Analyzer 35665A is used to produce the swept sine measurements across a range of frequencies, typically

from 0.1 Hz to 10.1 Hz. The range of frequencies, step size, and resolution are adjustable. Settling time as well as integration time can be regulated to average data over several periods at each individual frequency step. The HP Dynamic Signal Analyzer then compares the sine wave input into the speaker with the sinusoidally varying signal coming from the position of the Bragg spot. The analyzer generates a Bode diagram, which shows gain and phase versus swept frequencies.

Testing the setup

Using a mirror in place of the cuvette and adding weight to the turntable to keep the moment of inertia consistent with that of a cuvette, data was taken to test the mechanical resonance of the experimental setup as well as the coupling between the speaker and the turntable. As shown by the data (Figure 2), the mechanical resonance of the system was found to be at a frequency of 30.1 Hz. This is well above the frequencies that we will be looking at in this experiment.

The sensing error of the system was calculated to be 20 micron. This value for the error was arrived at by dividing the amplitude of the noise coming from the sensor by the amplitude of the signal coming from the sensor (Figure 3), and multiplying this by the amplitude of the laser beam sweeping across the sensor as it reflects off the mirror. This data was taken while the system was driving the turntable sinusoidally at a frequency of 1 Hz.

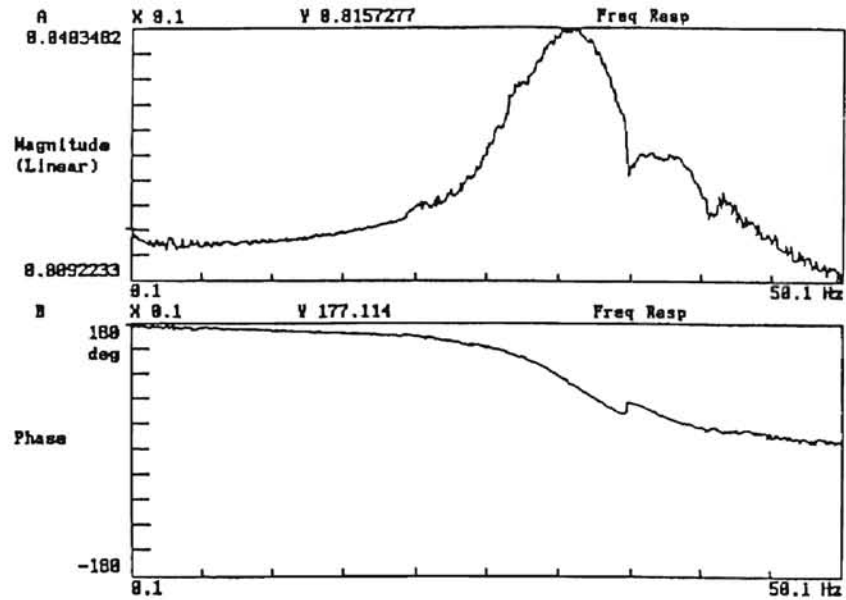


Figure 2. Mechanical resonance occurs at the gain peak (top) and correspondingly at phase shift of 90 degrees (bottom). Experimental data on the crystalline samples were taken in the frequency range of 0Hz to 5Hz, well below the mechanical resonance of the system.

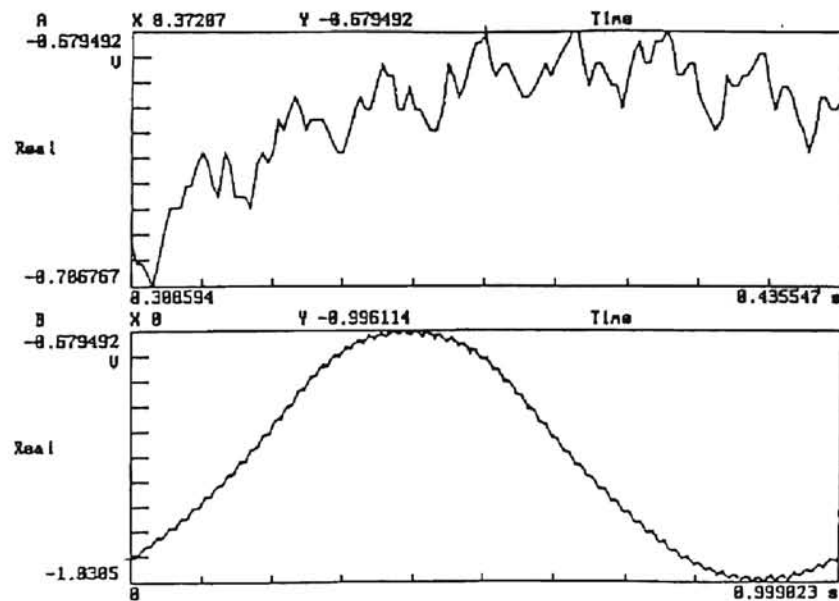


Figure 3. Sensing error is calculated by dividing the amplitude of noise (top) by the amplitude of signal (bottom) and multiplying by the amplitude of movement across the sensor. The above data is for the system being driven at 1Hz.

CHAPTER IV

RESULTS

Discussion of accuracy and reliability of resonance detection methods

Use of the position sensing detector had both good and bad points. The low sensing error provided excellent results during testing with a mirror. However, the detector was found to be sensitive to the size and shape of the incident Bragg spots. The signal from the detector is derived from the centroid of any light incident on its surface, so only one Bragg spot may be measured at a time. Multiple Bragg spots incident upon the sensor send a somewhat confused signal. As the sensor is moved farther from the sample, the amplitude of a spots movement increases but the size of the spot also increases. Therefore, before each swept sine measurement, the sample was driven at 1 Hz and the signal coming from the sensor was examined to ensure that it was sinusoidal and well defined. The location of the sensor could then be adjusted to maximize the clarity of the output signal.

As a measurement proceeded, a Bragg spot would often move off the position sensing surface, or disappear entirely. It is possible this movement could be caused by shearing within the sample destroying a crystal (shear melting), parking, or a crystal could be settling in the cuvette. While over the short term these effects are not noticeable, as typical measurement might take two hours to complete, almost half the measurements were incomplete and had to be redone.

Discussion of data fitting and results

Since there is a $1/n$ dependence in the amplitude (see Eq. 15), the $k_{l,0}$ gain peaks are the most readily seen. For each sample, the first prominent gain peak that corresponds to a phase shift of around 90 degrees on the Bode diagram

is taken to be the first resonance peak $k_{1,0}$. All other observed peaks are used as a measurement of accuracy (Figure 4). The error between the higher modes calculated from the position of the first resonance peak and the actual observed position was an average of 7.5%.

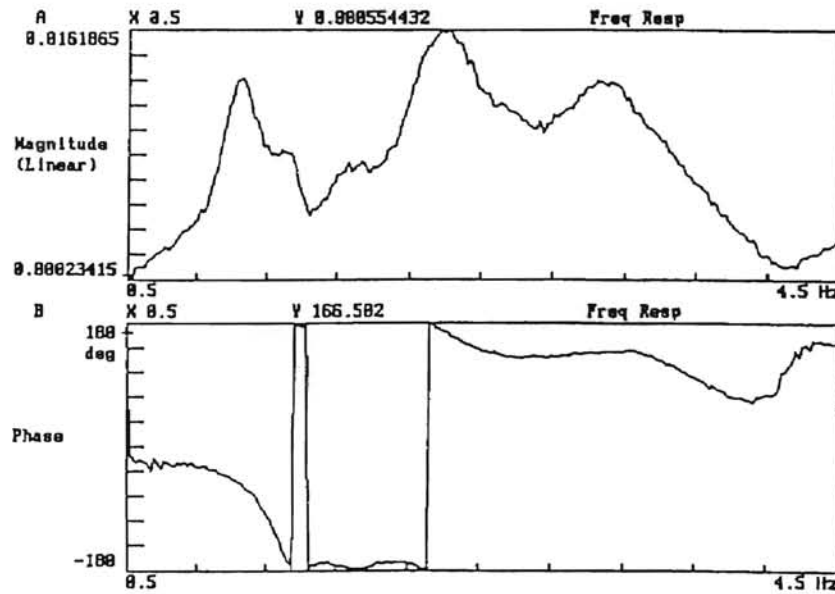


Figure 4. Typical Resonance Spectrum

By fitting the first observed amplitude peak to Equation 15 as in (Figure 5), we find that $k_{1,n}^2 \eta^2 / \rho^2$ is two orders of magnitude smaller than C_{tr}^2 . Therefore, the elastic modulus, G , is calculated from the first resonance peak using Eq. (18) and the definition of C_{tr} . Repeated measurements on a single sample taken several weeks apart, resulted in a difference in measurement of around 15%. One reason for this may be uncertainties in the ionic strength of the samples.

A plot of the elastic modulus for a range of volume fractions (Figure 6) shows the expected increase in elastic modulus as the volume fraction of particles increases. The data may deviate at smaller particle concentration due to the proximity of the liquid-crystal phase transition. At smaller concentrations than shown in the graph, the samples did not crystallize. These values for the elastic modulus are on the same order of magnitude as those measured by Palberg and Streicher[2].

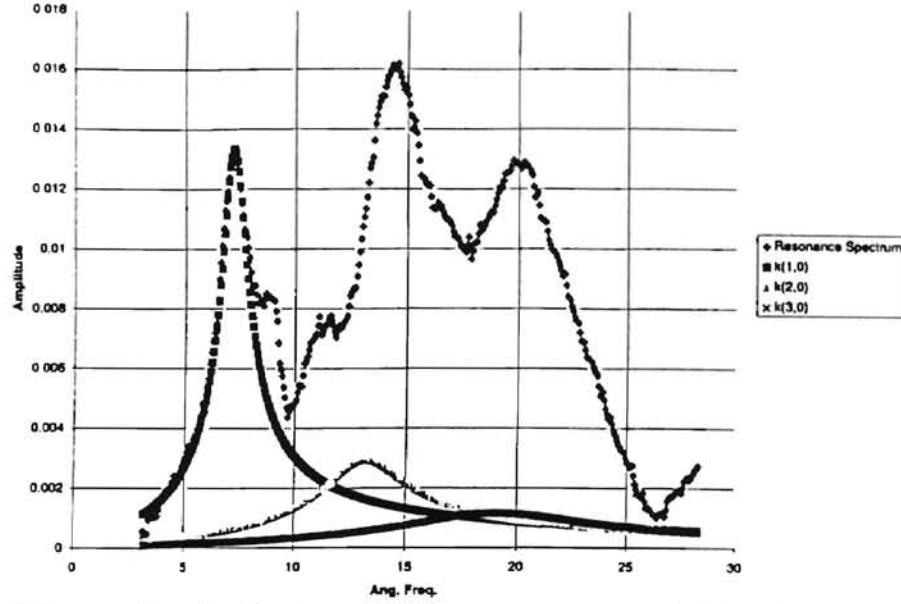


Figure 5. The amplitude of a typical resonance spectrum is fit to Eq. 15. $k_{l,n}^2 \eta^2 / \rho^2$ is found to be two orders of magnitude smaller than C_{tr}^2 .

With a comparison of the experimental data with a theoretical model developed by Buscall *et al.* [1], and based on the pair potential for interacting particles (see Appendix B), an experimental value for the number of screening ions in the sample can be determined. As shown by Figure 7 and Figure 8 a value of 125 ions or 150 ions can be measured depending on the whether the polystyrene forms a face-centered cubic (FCC) or body-centered cubic (BCC) array. From this an estimate of the particle's effective charge can be found to be around 2×10^{-17} coulombs.

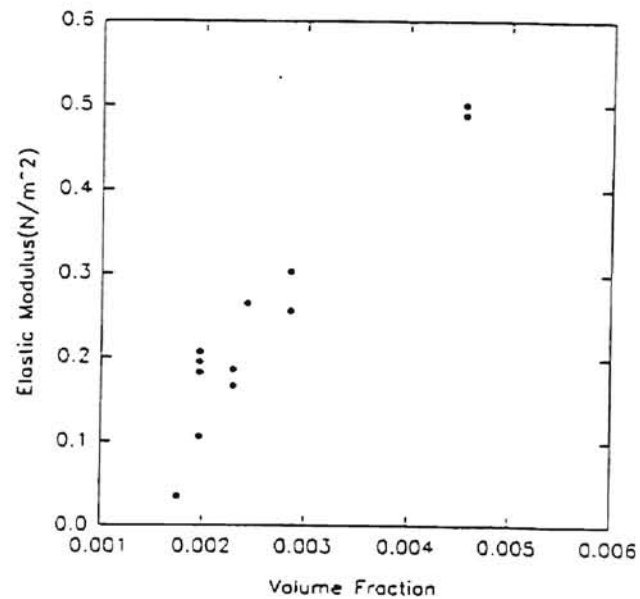


Figure 6. Elastic modulus vs. volume fraction for polystyrene sample. Particle diameter is 0.107micron.

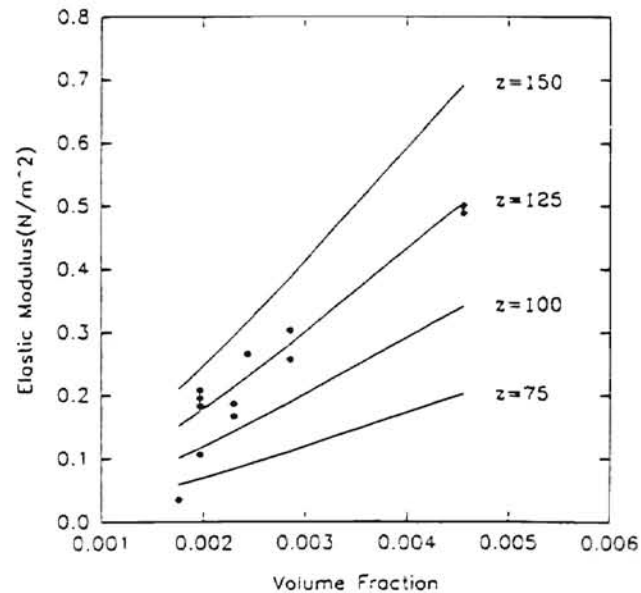


Figure 7. The solid lines indicate the theoretical relationship between elastic modulus and volume fraction in FCC crystals as described in Appendix B. Eq.(26), where z is the number of screening ions per polystyrene sphere.

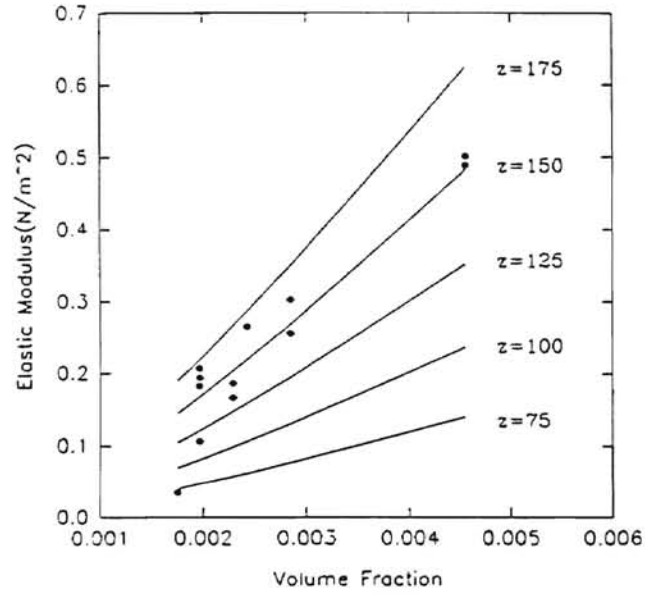


Figure 8. The solid lines indicate the theoretical relationship between elastic modulus and volume fraction in BCC crystals as described in Appendix B, Eq.(26), where z is the number of screening ions per polystyrene sphere.

CHAPTER V

CONCLUSIONS

It was demonstrated that the elastic modulus of a polystyrene lattice can be readily measured using the noninvasive Bragg scattering procedure detailed in this paper. The experimental data obtained using this measuring technique currently displays a relatively high error (15%). This is high when compared to 1% error obtained by Palberg *et al.* [3] or an estimated 5% error obtained by Dubois-Violette *et al.* [4], but indicates that with sample improvements, this system has the potential to be fine-tuned into a dependable method of measuring the elastic modulus of colloidal systems.

When everything in the system was working correctly, use of the position sensor resulted in an excellently resolved and sensitive data signal. A trade off existed, however, between averaging over several consecutive sets of data to obtain better results, and having the Bragg spot move off the sensor during longer measurement times. So, much still depends on the manual selection of a suitably stable and measurable Bragg spot.

BIBLIOGRAPHY

1. Buscall, R. *et al.* ; *J. Chem. Soc. , Faraday Trans.* **85**, 2889 (1982).
2. Palberg T. and Streicher K.; *Nature* **367**, 51 (1994).
3. Palberg, T. *et al.* ; *J. Phys. III France* **4**, 457 (1994).
4. Dubois-Violette, E. *et al.* ; *J. Phys. France* **41**, 369 (1980).
5. Nossal, R.; *J. Appl. Phys.* **50**, 3105 (1979).
6. Ackerson, B. J. Ed. ; *Phase Transitions* **21**, 73 (1990).
7. Lindsay H. M. and Chaikin P. M.; *J. Chem. Phys.* **76**, 3774 (1982).
8. Nossal, R. and Jolly, M.; *J. Appl. Phys.* **53**, 5518 (1982).
9. Landau, L. D. and Lifshitz, E. M., *Theory of Elasticity* (Addison-Wesley, Reading, Mass. , 1959).
10. Russel, W. B. and Benzing, D. W.; *J. Colloid Interface Sci.* **83**, 163 (1981).
11. Benzing, D. W. and Russel, W. B.; *J. Colloid Interface Sci.* **83**, 178 (1981).
12. Sommerfeld, A., *Mechanics of Deformable Bodies; Lectures in Theoretical Physics* (Academic, New York, 1950).
13. Hunter, R. J., *Zeta Potential in Colloidal Science* (Academic, London, 1981).
14. Russel, W. P. *et al.* *Colloidal Dispersions* (Cambridge University Press, 1989).
15. Kittel, Charles, *Introduction to Solid State Physics*, 6th ed (Wiley, New York, 1986)

APPENDICES

APPENDIX A

Amplification Circuitry

An amplification circuit diagram (Figure 9) was provided by UDT Sensors, Inc., however it was left to the author to determine the correct values of the components needed for the specific bandwidths involved in the experiment. In the first stage of the circuit, the raw signals from the anode and cathode connections on the sensor are amplified and compared to a reference circuit. The reference circuit has a bias adjustment to allow the positioning of a reference point on the sensor. Capacitors are present in the reference circuit to reduce AC noise and in the operational amplifier feedback loops to control bandwidth. At the second stage of the circuit, the anode and cathode signals are put through difference amplifiers as well as a sum amplifier. Finally, the differentiated signals are divided by the summed signals, giving output data for both the x and y axis.

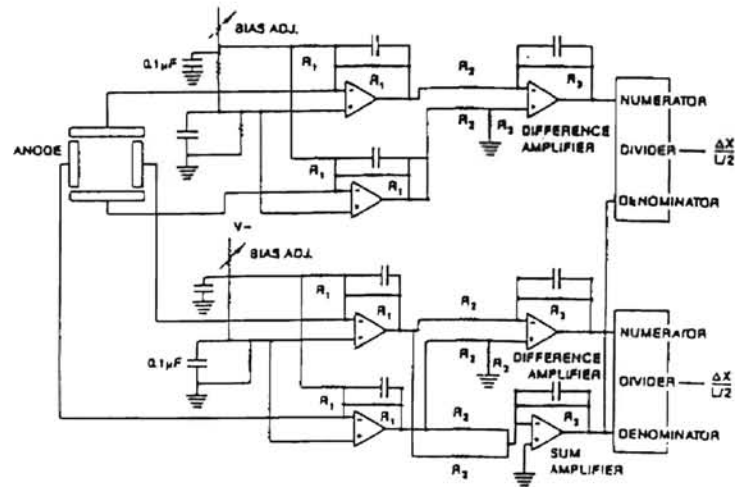


Figure 9. Circuit Diagram

APPENDIX B

Theoretical Shear Modulus

At the low electrolyte concentrations and volume fractions used in this experiment, the pair potential for interacting particles will be dominated by the electrostatic repulsion, V_R , due to overlapping of electrical double layers. For a sample made of spherical particles of radius a , with a separation distance R and a diffuse layer potential ψ_d , then the electrostatic repulsion can be written as[1]

$$V_R = \frac{4\pi\epsilon\epsilon_0 a^2 \psi_d^2}{R} \exp[-\kappa(R - 2a)] \quad (20)$$

where ϵ is the permittivity of the medium, ϵ_0 is the permittivity of free space, and ψ_d is given by[13]

$$\psi_d = \frac{ze}{4\pi\epsilon\epsilon_0} [a + a^2\kappa]^{-1} \quad (21)$$

where z is the number of screening ions per polystyrene sphere. The Debye-Hückel reciprocal double-layer thickness parameter, κ , is defined as[14]

$$\kappa = \left(\frac{e^2 Z^2 n_b}{\epsilon\epsilon_0 kT} \right)^{\frac{1}{2}} \quad (22)$$

where Z is the valence of the electrolyte, k is Boltzmann's constant, T is the temperature, and n_b is

$$n_b = \frac{z\phi}{\frac{4}{3}\pi a} \quad (23)$$

Eq.(20) is applicable only under the condition that the particles interact at a constant diffuse double-layer potential and $\kappa a < 3$ [1].

The particle separation in an ordered array can be related to the volume fraction by[1]

$$R = 2a \left(\frac{\phi_m}{\phi} \right)^{\frac{1}{3}} \quad (24)$$

where ϕ is the volume fraction and ϕ_m is the packing fraction. ϕ_m is 0.74 for face-centered cubic (fcc) arrays and 0.68 for body-centered cubic (bcc) arrays[15].

The shear modulus can be expressed in terms of the total energy of interaction by[1]

$$G_0^{th} = \frac{\alpha}{R} \left(\frac{\partial^2 V_T}{\partial R^2} \right) \quad (25)$$

where V_T is the total energy of interaction and $\alpha = (3/32)\phi_m n$. n is the number of nearest neighbors. The subscript zero indicates that this is the high-frequency limit as relaxation was not considered. Since electrostatic repulsion dominates the particle interactions, V_T in Eq.(25) can be replaced by V_R .

Differentiating Eq.(15) twice and putting the result in Eq.(25) yields a theoretical shear modulus of[1]

$$G_0^{th} = 4\pi\alpha\epsilon\epsilon_0 a^2 \psi_d^2 \left(\frac{\kappa^2 R^2 + 2\kappa R + 2}{R^4} \right) \exp[-\kappa(R - 2a)] \quad (26)$$

for $\kappa a < 3$.

2

VITA

GREGORY LEE TRELEVEN

Candidate for the Degree of

Master of Science

Thesis: MEASUREMENT OF THE ELASTIC MODULUS IN COLLOIDAL
CRYSTALS USING A BRAGG SCATTERING TECHNIQUE

Major Field: Physics

Biographical:

Personal Data: Born in Cudahy, Wisconsin, on September 26th 1968, the son of Gary and Leslie Treleven.

Education: Graduated from Mustang High School, Mustang, Oklahoma, May, 1987; received a Bachelor of Science degree at Oklahoma State University, Stillwater, Oklahoma, May, 1992; completed the requirements for the Master of Science Degree at Oklahoma State University, Stillwater, Oklahoma, August 1997.